Observation of g/u-symmetry mixing in the high-n Rydberg states of HD

Author(s):
Sprecher, Daniel; Merkt, Frédéric

Publication date:
2014-03

Permanent link:
https://doi.org/10.3929/ethz-b-000083384

Originally published in:
The Journal of Chemical Physics 140(12), https://doi.org/10.1063/1.4868024

Funding acknowledgement:
149216 - Zeeman and Stark deceleration of atoms and molecules (SNF)

The following article appeared in *J. Chem. Phys.* **140**, 124313 (2014) and may be found at http://dx.doi.org/10.1063/1.4868024.

Effects of *g/u*-symmetry mixing in the high-n Rydberg states of HD

Daniel Sprecher and Frédéric Merkt*

Laboratorium für Physikalische Chemie,

ETH-Zürich, 8093 Zürich, Switzerland

(Dated: November 19, 2019)

Abstract

The structure and dynamics of high-np Rydberg states converging to the $(v^+ = 0, N^+ = 1)$ level of the $X^+\,^2\Sigma_g^+$ electronic ground state of HD^+ were studied under field-free conditions. The singlet $61p1_2$ Rydberg state of *ungerade* symmetry was observed to autoionize with a lifetime of 77(10) ns, which can only take place when *g/u* symmetry is broken by emission of a d electron. Shifts induced by *g/u*-symmetry mixing of up to 20 MHz were observed for members of the $np1_1$ Rydberg series which lie close to $nd2_1$ Rydberg states. From these shifts, the magnitude of the off-diagonal eigenquantum-defect element $\mu_{pd} = 0.0023(3)$ of singlet-π symmetry was determined and the corresponding autoionization dynamics could be characterized. The ionization energy of the GK $(v = 1, N = 1)$ state of HD was measured to be 12 710.544 23(10) cm^{-1}.

PACS numbers: 33.80.Rv, 33.80.Eh, 33.20.Wr, 33.15.Ry, 32.80.Zb, 31.30.Gs

* frederic.merkt@phys.chem.ethz.ch

I. INTRODUCTION

Within the Born-Oppenheimer (BO) approximation, all isotopomers of molecular hydrogen share the same electronic wave functions and their electronic structures are therefore identical [1]. The BO electronic wave functions are either symmetric (label g for *gerade*) or antisymmetric (label u for *ungerade*) with respect to the inversion at the center of charge. Because of the mass asymmetry of the heteronuclear isotopomer HD, its exact wave functions can exhibit a mixing of g and u symmetry. The most prominent effect of this mixing is the existence of a small permanent electric dipole moment of about 0.001 Debye in the ground state [2–4]. This dipole moment can be interpreted as arising from a weak interaction of the $X\,^1\Sigma_g^+$ ground state with excited states of $^1\Sigma_u^+$ and $^1\Pi_u^+$ symmetry [5]. The interaction also shifts the ground state of HD to lower energies by $0.05\,\mathrm{cm}^{-1}$ [6, 7] and needs to be considered when calculating the rovibrational structure and the dissociation energy of HD at high precision [8].

Cases of strong g/u-symmetry mixing in HD have been observed in the low-lying electronically excited states. States of approximate g symmetry were observed to decay back to the $X\,^1\Sigma_g^+$ ground state in a fast single-photon process [9, 10] and level shifts of up to $10\,\mathrm{cm}^{-1}$ were identified [11, 12]. The observation of additional lines and irregular spectral patterns render the spectra of HD much more difficult to analyze than those of H_2 and D_2 [9, 13, 14]. The effects of g/u-symmetry mixing were found to be particularly pronounced near the $n = 2$ dissociation limit, where states of g and u symmetry systematically are almost degenerate [15, 16].

Other energetic regions where *gerade* and *ungerade* states lie in close proximity are the regions near ionization thresholds, where the density of high-n Rydberg states is very high. For these states, the effects of g/u-symmetry mixing have to our knowledge not yet been systematically investigated. Most treatments of high-n Rydberg states of HD neglected such a mixing and nevertheless found good agreement with experimental results [17–21]. Although these studies indicate that g/u-symmetry mixing is weak, there is also experimental evidence for perturbations. In Ref. [22], $N^+ = 1$ Rydberg states of HD were observed to autoionize into the $N^+ = 0$ continuum on a timescale of less than 1 µs which can only take place if g/u symmetry is broken. However, because these measurements were preformed in the presence of a small electric field (of 0.7 V/cm), it was not possible to rule out that the observed

g/u-symmetry breaking was induced by the field. The goal of the investigation presented in this article was to investigate the effects of g/u-symmetry mixing on the structure and dynamics of high-n Rydberg states of HD more systematically than in previous studies and under field-free conditions.

II. EXPERIMENTAL

The singlet np Rydberg states around $n = 60$ converging to the vibrational and electronic ground state of HD^+ were excited using the triply resonant excitation scheme

$$X\,(v=0,N=1) \xrightarrow{\text{VUV}} 2\text{p}\sigma\,B\,(v=4,N=2) \xrightarrow{\text{VIS}} 3\text{d}\sigma\,GK\,(v=1,N=1) \xrightarrow{\text{NIR}} n\text{p}1_{1,2}. \quad (1)$$

The notation $n\,\ell\,N_N^+$ is used to label the high-n Rydberg states, where n is the principal quantum number, ℓ is the orbital angular-momentum quantum number of the Rydberg electron, N^+ is the rotational quantum number of the HD^+ ion core, and N is the total angular-momentum quantum number without spins ($\vec{N} = \vec{N}^+ + \vec{\ell}$).

The experimental setup and the vacuum-ultraviolet (VUV), visible (VIS), and near-infrared (NIR) laser systems were identical to these used in our previous study on the np Rydberg states of H_2 [23]. The VUV radiation (wavelength 105.5 nm, bandwidth $\sim$10 GHz, pulse energy $\sim$1 nJ) was produced by resonance-enhanced sum-frequency mixing in xenon using two commercial Nd:YAG-pumped dye lasers. The VIS radiation (wavelength 588.2 nm, bandwidth $\sim$3 GHz) was generated with a third commercial dye laser pumped by the same Nd:YAG laser. Pulse energies of less than 10 μJ were used for the VIS radiation to avoid the generation of HD^+ ions by a resonance-enhanced two-photon ionization process from the $B\,(v=4,N=2)$ state. For the generation of near-Fourier-transform-limited NIR pulses with wavelengths around 788.6 nm, the Ti:Sa laser system described in Ref. [24] was used. In brief, weak pulses, generated from the continuous-wave (cw) output of a Ti:Sa ring laser using an acousto-optical modulator (AOM), were amplified to pulse energies of $\sim$40 μJ using a multipass pulse amplifier. The lengths of the NIR pulses could be varied in the range 10–10^3 ns depending on whether time- or frequency-resolved measurements were carried out.

A schematic diagram of the vacuum chamber in which the laser excitation was carried out is presented in Fig. 1. A supersonic beam of HD molecules was formed using a pulsed valve

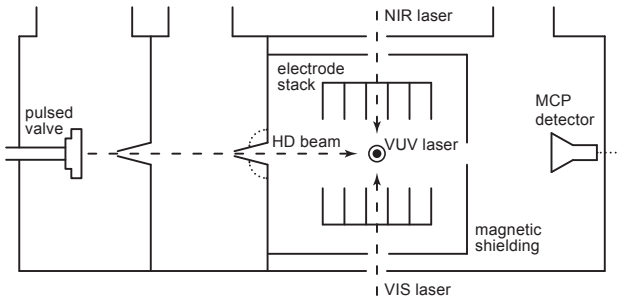

FIG. 1. Schematic diagram of the experimental chamber (not to scale).

operated at a stagnation pressure of 3 bar and a repetition rate of 25 Hz. Two consecutive skimmers, the second of which was adjusted and aligned from outside the vacuum chamber, were used to select a sample of HD molecules having a narrow velocity distribution in the propagation direction of the NIR laser beam. The molecules were excited in the center of a cylindrically symmetric electrode stack consisting of six resistively coupled metallic plates designed for the application of homogeneous electric fields. The three laser beams used to excite high-np Rydberg states intersected the molecular beam at right angles, as shown in Fig. 1. The laser-excitation region was surrounded by two concentric mumetal tubes to suppress inhomogeneous stray magnetic fields.

For the detection of high-n Rydberg states, an electric field with an amplitude of 70 V/cm and a rise time of ~ 50 ns was applied typically 100 ns after laser excitation. The electric field ionized the Rydberg states and accelerated the HD^+ ions toward a microchannel plate detector where they impinged after a time of flight of about 2 µs. The spectra were obtained by monitoring the HD^+ ion signal as a function of the NIR laser frequency.

The NIR laser frequency was calibrated using a fraction of the cw output of the Ti:Sa ring laser. Doppler-free saturation spectroscopy of I_2 was used for the determination of absolute frequencies. The transition frequencies of the $X\,(v'' = 14\text{–}15, J'') \rightarrow B\,(v' = 0, J')$ transitions of $^{127}I_2$, which are known with an accuracy of better than 0.1 MHz, were taken from Ref. [25]. The relative frequency calibration was achieved using a high-finesse etalon locked to a HeNe laser. The free spectral range (FSR) of the etalon was measured daily by recording several Doppler-free iodine lines separated by up to 1 THz (30 cm^{-1}) simultaneously with the etalon traces. The resulting values of the FSR were centered around 149.967 MHz and had uncertainties of 0.4 kHz.

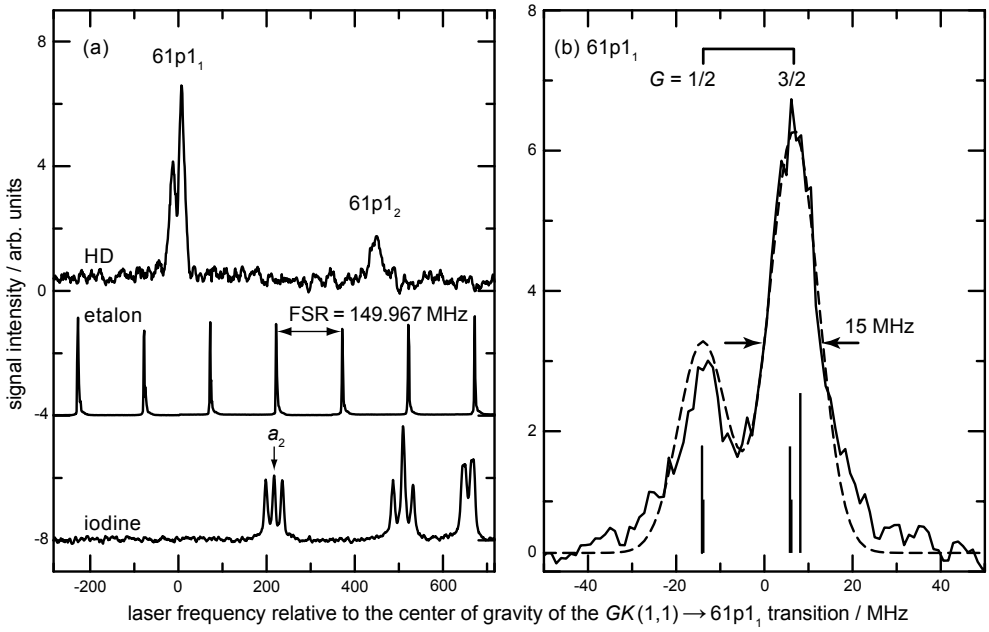

FIG. 2. (a) Observed spectrum of the $GK\,(v=1, N=1) \rightarrow 61\mathrm{p}1_N\,(N=1,2)$ transitions of HD near $12\,681.1\,\mathrm{cm}^{-1}$. For the frequency calibration, etalon traces and iodine spectra were recorded simultaneously with the HD spectra (shifted along the vertical axis for clarity). (b) Experimental (full line) and simulated (dashed line) spectrum of the $N=1$ orbital-fine-structure component of the $61\mathrm{p}1_N$ Rydberg state. The stick spectrum corresponds to the calculated hyperfine structure.

III. RESULTS

A. Observed fine and hyperfine structures

The observed spectrum of HD near the $GK\,(v=1, N=1) \rightarrow 61\mathrm{p}1_1$ transition is displayed in Figure 2a together with the etalon transmission spectrum and the Doppler-free iodine spectrum used for calibration. The $N=1$ and $N=2$ orbital-fine-structure components of the $61\mathrm{p}1_N$ Rydberg state are separated by 450 MHz and both are observed in Figure 2a. The observed Doppler-free iodine lines shown in Figure 2a are assigned to the a_1–a_{11} hyperfine components of the $X\,(v''=14, J''=155) \rightarrow B\,(v'=0, J'=154)$ transition in $^{127}\mathrm{I}_2$. For the absolute frequency calibration, the a_2 hyperfine component located at $12\,681.112\,828(3)\,\mathrm{cm}^{-1}$ (380.170 1985(1) THz [25]) was used.

The $GK\,(v=1, N=1) \rightarrow 61\mathrm{p}1_1$ transition, shown on an enlarged scale in Figure 2b, reveals a splitting of 21 MHz which is assigned to the $G = 1/2$ and $G = 3/2$ main hyperfine

components. The complete hyperfine structure of the $61p1_1$ Rydberg state was calculated in Ref. [26] and is shown as stick spectrum in Figure 2b. To determine the transition frequency of the $GK\,(v = 1, N = 1) \rightarrow 61p1_1$ transition, the lineshape was modeled using four fit parameters by convoluting the calculated stick spectrum with a Gaussian line-shape function. The fit parameters were the central position of the stick spectrum, the width and amplitude of the Gaussian function, and a constant background. The simulated (dashed line in Figure 2b) and observed spectra (full line) are in excellent agreement, indicating that the hyperfine structure calculated in Ref. [26] is correct. The full width at half maximum (FWHM) of the observed transitions is limited to 15 MHz by Doppler broadening.

The spectrum of the $GK\,(v = 1, N = 1) \rightarrow 61p1_2$ transition shown in Figure 2a does not exhibit any splitting. This is consistent with the MQDT calculations of Ref. [26] which predict a main hyperfine splitting of only 13 MHz for the $61p1_2$ Rydberg state, *i.e.*, too small to be resolved in the current experiment. The reason for the reduced hyperfine splitting of the $N = 2$ orbital-fine-structure component compared to the $N = 1$ component is a strong rotational channel interaction with the $21p3_2$ Rydberg state. The exchange interaction, which is larger at $n = 21$ than at $n = 61$, opposes the hyperfine interaction so that admixture of low-n character to the $61p1_2$ Rydberg state reduces the hyperfine splitting. The $61p1_1$ Rydberg state is not subject to a similar rotational channel interaction because the $np3_N$ Rydberg series does not possess an $N = 1$ component.

B. Field-induced *g/u*-symmetry mixing

High-n Rydberg states are very sensitive to electric fields and stray electric fields of only a few mV/cm are sufficient to significantly perturb Rydberg states around $n = 50$. The Stark structure of high-n Rydberg states, *i.e.* the energy shifts and splittings induced by dc electric fields, can be calculated accurately using a combination of MQDT and the method described in Refs. [27–29]. For this purpose, spins are ignored and a Hamiltonian matrix in Hund's case (d) is constructed. The basis is restricted to Rydberg states with $N^+ = 1$ and $n = 59$–63. The diagonal elements of the Hamiltonian matrix are given by the field-free energies of the corresponding Rydberg states, which, for the np Rydberg states, were taken from the MQDT results reported in Ref. [26]. For the ns, nd, and nf Rydberg states, MQDT calculations ignoring spins were performed using the eigenquantum defects from Ref. [30]

(for the ns and nd Rydberg states) and Ref. [31] (for the nf Rydberg states). For the nonpenetrating Rydberg states with $\ell > 3$, the quantum defects were set to 0.

The presence of an electric field of amplitude F leads to nonzero off-diagonal elements in the Hamiltonian matrix which are given by [28]

$$\left\langle \nu\ell N^+ N M_N \right| eFz \left| \nu'\ell' N^{+\prime} N' M'_N \right\rangle = eF\delta_{M_N M'_N}\delta_{N^+ N^{+\prime}}(-1)^{N-M_N+N'+N^++\ell+1} \times \sqrt{(2N+1)(2N'+1)} \begin{pmatrix} N & 1 & N' \\ -M_N & 0 & M_N \end{pmatrix} \begin{Bmatrix} \ell & N & N^+ \\ N' & \ell' & 1 \end{Bmatrix} \langle \nu\ell||r||\nu'\ell'\rangle. \quad (2)$$

In Eq. (2), ν is the effective principal quantum number with respect to the $N^+ = 1$ threshold and M_N is the projection quantum number of $\vec{N}$ onto the electric field axis (the z axis). The last factor in Eq. (2) is a reduced matrix element which was calculated numerically as described in Refs. [28, 29]. The expression given on the right-hand side of Eq. (2) can only be nonzero if $|\ell - \ell'| = 1$. The field therefore mixes states of opposite g/u symmetry and of opposite parity.

Having constructed the Hamiltonian matrix including the dc Stark effect, the energy level structure is obtained by diagonalization. The calculated Stark structure at $n = 61$ is depicted as a function of the electric-field amplitude in Figure 3 and the $|M_N| = 0, 1,$ and 2 Stark states are shown as solid, dashed, and dotted lines, respectively. For the $61p1_1$ and $61p1_2$ Rydberg states observed in Figure 2, the splittings and shifts were measured for several intentionally applied dc electric fields and are depicted in Figure 3b as full circles. From the comparison of the experimental to the calculated Stark structures in Figure 3b, one can deduce that a dc electric field of 1.9(4) mV/cm needs to be applied to compensate the stray electric field present in the excitation region. In this way, only the stray electric field in the propagation direction of the HD beam is compensated (see Figure 1). The cylindrical geometry of the electrode stack ensures, however, that the stray electric field in all other directions is sufficiently small to have a negligible effect on the structure of $\ell \leq 3$ Rydberg states around $n = 60$. After field compensation, g/u-symmetry mixing induced by the stray fields is negligible.

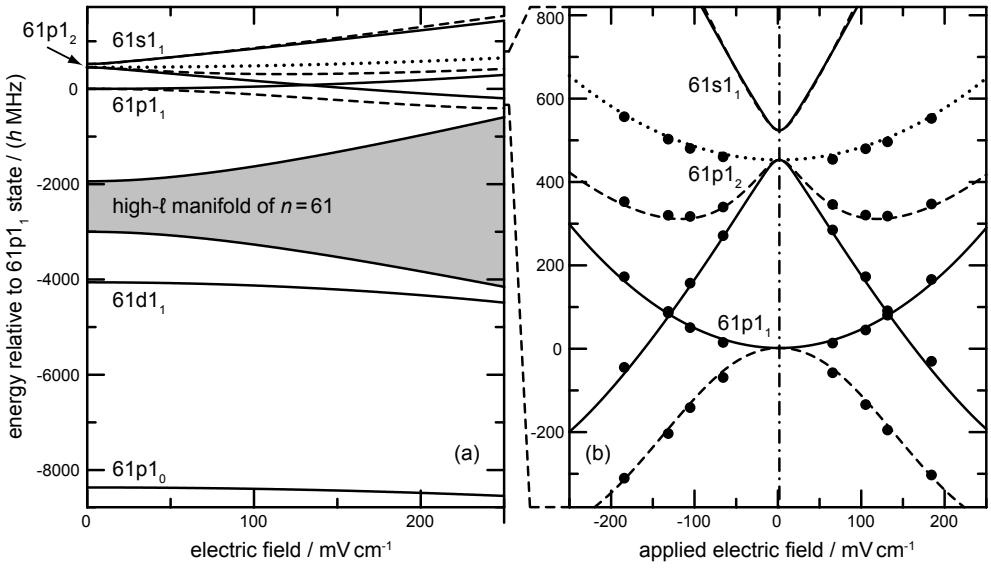

FIG. 3. (a) Calculated dc Stark shifts and splittings of all singlet Rydberg states near $n = 61$ converging to the $(v^+ = 0, N^+ = 1)$ state of HD^+. Stark states with $|M_N| = 0, 1$, and 2 are shown as solid, dashed, and dotted lines, respectively. The area shaded in gray contains a dense manifold of Stark states with main contributions of states with ℓ values between 2 and 60. In panel (b), the calculated dc Stark map is compared to the measurements (shown as full circles) in the region of the $61p1_1$ $(S = 0, v^+ = 0)$ Rydberg state. The dash-dotted vertical line indicates the electric field of 1.9(5) mV/cm which compensates the stray electric field present in the excitation region.

C. Autoionization dynamics of $N^+ = 1$ Rydberg states

The time-of-flight spectra of HD^+ observed after tuning the NIR laser frequency to excite the $N = 1$ and $N = 2$ orbital-fine-structure components of the $61p1_N$ Rydberg state are depicted in Fig. 4 as solid lines. In these measurements, the energies of the VIS laser pulses were increased to about 50 μJ and the pulse length of the NIR radiation was reduced to less than 20 ns. The profiles represented as dashed lines, with maxima at 2.20 μs, correspond to prompt HD^+ ions produced by the VIS radiation in a resonance-enhanced two-photon ionization process from the $B\,(v = 4, N = 2)$ state. The time-of-flight spectra obtained following excitation to the $61p1_1$ Rydberg state have their maxima shifted to later times (~ 2.21 μs) because the ions must first be produced at a finite electric field strength when the delayed (Δt) ramped electric-field pulse is applied. Compared to prompt ions, they thus arrive at later times at the detector. The profiles recorded for $\Delta t = 28$ ns and $\Delta t = 138$ ns

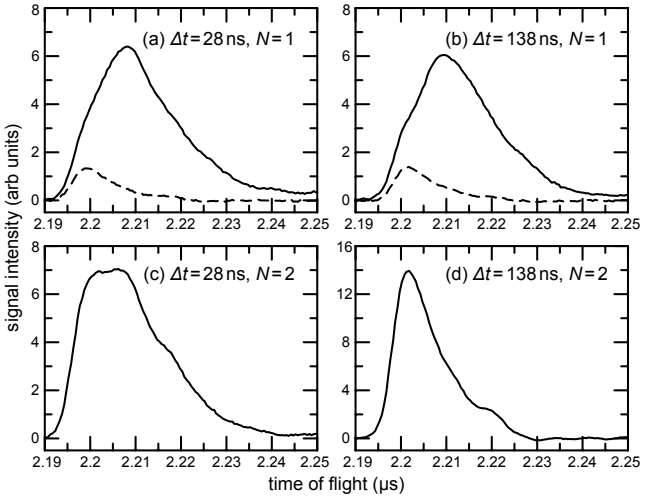

FIG. 4. HD^+ time-of-flight spectra observed for the specified delay between laser excitation and pulsed-field ionization (Δt) and after tuning the NIR laser frequency to the specified N component of the $GK \rightarrow 61p1_N$ transition. The dashed lines depict the observed spectra when the NIR laser was blocked.

shown in panels (a) and (b) of Fig. 4 do not significantly differ, indicating that the $61p1_1$ Rydberg state has a lifetime much longer than 138 ns. For the time-of-flight spectra obtained after excitation to the $61p1_2$ Rydberg state (see panels (c) and (d) of Fig. 4), more HD^+ ions are observed at the same flight time as the prompt ions (2.20 μs) when the delay is increased. This observation can only be explained by an autoionization process of the $61p1_2$ Rydberg state into the $N^+ = 0$ continuum taking place during the field-free period between the laser pulse and the application of the pulsed electric field. One an therefore conclude that $\Delta N^+ = -1$ rotational autoionization of the $61p1_2$ state takes place within $\sim$100 ns and that of the $61p1_1$ state is forbidden.

Rotational autoionization of $N^+ = 1$ Rydberg states in H_2 and D_2 is forbidden because it could only take place to $N^+ = 0$ continua for energetic reasons and thus represents a transition between *ortho* and *para* spin isomers. In HD, the autoionization of a $np N^+$ state to an $\varepsilon p N^+ - 1$ continuum is forbidden by symmetry because the change of N^+ by an odd integer inverts the rotational parity. $\Delta N^+ = -1$ autoionization processes in np Rydberg states of HD are therefore only possible if the electronic parity is inverted and the electron is emitted as a partial wave with an even value of ℓ, therefore conserving the total parity but breaking g/u symmetry. An energy level diagram of all relevant Rydberg

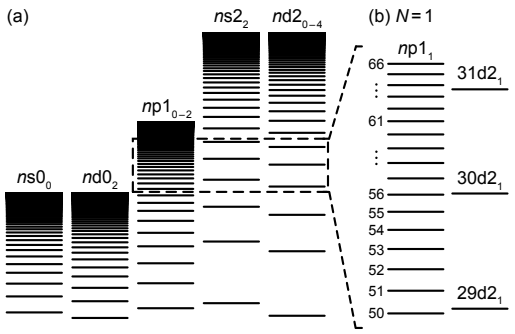

FIG. 5. (a) Schematic energy level diagram of the singlet ns, np, and nd Rydberg states of HD with positive parity in the region of the $X^+\,^2\Sigma_g^+$ ($v^+ = 0$) threshold. The $N = 1$ Rydberg states are shown on an enlarged scale in panel (b).

states of positive total parity is presented in Figure 5a. When neglecting the effect of spins and in the absence of electric fields, the autoionization process must conserve the quantum number N. Consequently, the autoionization of the $61p1_2$ Rydberg state into the $\varepsilon d0_2$ continuum observed in panels (c) and (d) of Fig. 4 requires g/u-symmetry breaking, but is otherwise allowed by both parity ($+ \leftrightarrow +$) and angular-momentum ($\Delta N = 0$) conservation rules. In contrast, for the $61p1_1$ Rydberg state, there are no continua of the appropriate symmetry under field-free conditions because s and d channels with $N^+ = 0$ have $N = 0$ and 2, respectively. Consequently, autoionization is forbidden by the $DeltaN = 0$ angular-momentum conservation rule, in agreement with the observations presented in panels (a) and (b) of Fig. 4.

To determine the autoionization lifetime of the $61p1_2$ Rydberg state, the fraction of neutral Rydberg states present in the sample at the time of pulsed-field ionization was measured for different delays Δt. The shape of time-of-flight spectra originating from a pure sample of HD^+ ions is known from the measurement of the prompt ions only (dashed lines in Figure 4) and the shape of the time-of-flight spectra corresponding to the field ionization of long-lived Rydberg states corresponds to that obtained for the $61p1_1$ Rydberg state which cannot decay by autoionization as just explained ,*i.e.*, to the difference between the solid and dashed lines in Figures 4a and 4b. The time-of-flight spectra of the $61p1_2$ Rydberg state can therefore be reconstructed as illustrated in Figures 6a and 6b. In these figures, the solid lines represent the normalized experimental time-of-flight spectra of the $61p1_2$ Rydberg state after subtraction of the prompt ion signal and the two dashed lines the

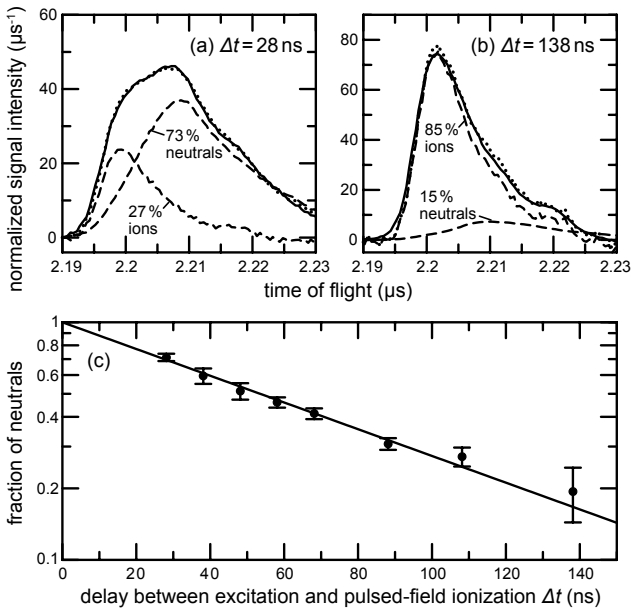

FIG. 6. In panels (a) and (b), the observed (solid lines) and simulated (dotted lines) time-of-flight spectra of the $61p1_2$ Rydberg states are shown for $\Delta t = 28\,\text{ns}$ and $\Delta t = 138\,\text{ns}$, respectively. The contributions to the simulated time-of-flight spectra from neutral and ionized Rydberg states are depicted as dashed lines. In panel (c), the observed fraction of neutral Rydberg states (full circles) together with their uncertainties (vertical lines) are shown on a logarithmic scale as a function of Δt. The solid line represents the result of an exponential fit to the observed values and its lifetime is $\tau = 77(10)\,\text{ns}$.

contributions form the prompt ion signal and the field ionization signal. The dotted lines represent the result of the simulation where the fraction of Rydberg states present in the sample at the time of field ionization was used as the only fit parameter. The agreement between solid and dotted lines is excellent and leaves no doubt concerning the validity of the signal reconstruction procedure. This procedure was repeated for several time delays Δt and on different days and the results are summarized in Fig. 6c. The experimental results are compatible with a single exponential decay, and the $1/e$-lifetime of the $61p1_2$ Rydberg state is $\tau = 77(10)\,\text{ns}$.

D. Observed shifts in the $n\mathrm{p}1_1$ Rydberg series

The $n\mathrm{p}1_1$ Rydberg states of HD around $n = 60$ form a regular Rydberg series, *i.e.*, their spectral positions $\tilde{\nu}_n$ relative to the $N^+ = 1$ ionization threshold are well described by Rydberg's formula

$$\tilde{\nu}_n = -\frac{\mathcal{R}_{\mathrm{HD}}}{(n - \bar{\mu})^2}. \tag{3}$$

In Eq. (3), $\mathcal{R}_{\mathrm{HD}} = 109\,717.395\,\mathrm{cm}^{-1}$ is Rydberg's constant adapted to the mass of HD and $\bar{\mu}$ is the effective quantum defect. The values of $\bar{\mu}$ are to a first approximation independent of n ($\bar{\mu} \approx -0.082$). Accurate values of $\bar{\mu}$ were determined in Ref. [26] using multichannel quantum-defect theory (MQDT).

To detect a possible perturbation caused by *g/u*-symmetry mixing, the positions of all $n\mathrm{p}1_1$ Rydberg states with $n = 50$–66 were measured relative to the position of the $61\mathrm{p}1_1$ state. The results are listed in the second column of Table I and their uncertainties are estimated to be 3 MHz, limited by the statistical uncertainty caused by the Doppler-limited linewidth of 15 MHz (full width at half maximum). In the third column of Table I, the observed positions are compared to the relative positions (taken from Ref. [26]) calculated without consideration of *g/u*-symmetry mixing. The agreement between observed and calculated positions is excellent, except for the $56\mathrm{p}1_1$ Rydberg state which is observed 20 MHz lower than predicted by the calculations. This deviation is too large to be an artefact and must arise from an interaction with a nearby Rydberg state of the same parity and N value.

The observed spectrum of HD in the region of the $GK \rightarrow 56\mathrm{p}1_1$ transition is depicted in Fig. 7. Between 1.5 and 2.7 GHz above the strong transition to the $56\mathrm{p}1_1$ Rydberg state, several weak transitions are observed. These transitions are represented on a larger scale in the inset of Fig. 7. Our calculations do not predict any np or nf Rydberg state of *ungerade* symmetry in this region. The *gerade* $n\mathrm{d}2_1$ Rydberg states form a regular Rydberg series with $\bar{\mu} \approx 0.045$ converging to the $N^+ = 2$ threshold (see Fig. 5b). The $30\mathrm{d}2_1$ is calculated to lie 2.1 GHz above the $56\mathrm{p}1_1$ Rydberg state and the weak transitions visible in Fig. 7 are therefore assigned to the $GK \rightarrow 30\mathrm{d}2_1$ transition. The observed splitting is in agreement with the main hyperfine interval of HD^+ [32] (see inset of Fig. 7). Because the exchange interaction in high-nd Rydberg states is smaller than the hyperfine interaction, the $30\mathrm{d}2_1$ Rydberg state must exhibit a hyperfine structure very similar to that of HD^+.

TABLE I. Comparison between observed and calculated relative transition frequencies to members of the $n\mathrm{p}1_1$ Rydberg series. All values are given in units of MHz and for the center of gravity of the hyperfine components.

n	ν_{obs}	o−c[a]	$\Delta\nu_{g/u}$[b]	o−c$_{g/u}$[c]
50	−429 831.4	−3.6	−6.6	2.1
51	−378 976.8	5.8	1.5	3.4
52	−331 036.0	1.9	0.5	0.5
53	−285 774.2	2.9	0.1	1.9
54	−243 000.2	3.6	−0.3	3.0
55	−202 542.1	−4.1	−1.0	−4.0
56	−164 238.4	−20.1	−20.7	−0.3
57	−127 891.4	3.3	1.2	1.2
58	−93 427.5	3.4	0.5	2.0
59	−60 704.0	−1.4	0.2	−2.5
60	−29 588.6	4.4	0.0	3.5
61	0	0	−0.2	−0.7
62	28 175.0	0.3	−0.5	−0.1
63	55 016.9	−3.4	−1.7	−2.6
64	80 621.1	2.0	2.8	−1.7
65	105 045.9	−1.2	0.7	−2.8
66	128 373.7	−0.8	0.4	−2.1
			Standard deviation:	2.4

[a] Difference between observed and calculated frequencies when neglecting g/u-symmetry mixing.

[b] Calculated shifts induced by g/u-symmetry mixing.

[c] Difference between observed and calculated frequencies when accounting for g/u-symmetry mixing (relative to mean value, *i.e.*, shifted by −0.9 MHz).

E. A simple MQDT treatment of g/u-symmetry mixing

To quantitatively analyze the electronic channel interaction between the otherwise regular $n\mathrm{p}1_1$ and $n\mathrm{d}2_1$ Rydberg series we use two-channel quantum-defect theory. Spins can be

neglected in the treatment to a good approximation because the separation between all Rydberg states is larger than the hyperfine splittings. The positions of the perturbed Rydberg states can be parametrized by the simple quantization condition [33]

$$\det \begin{vmatrix} \tan \pi\nu_1(E) + \tan \pi\mu_{\rm pp} & \tan \pi\mu_{\rm pd} \\ \tan \pi\mu_{\rm pd} & \tan \pi\nu_2(E) + \tan \pi\mu_{\rm dd} \end{vmatrix} = 0, \qquad (4)$$

In Eq. (4), $\nu_1(E)$ and $\nu_2(E)$ are the effective principal quantum numbers with respect to the $N^+ = 1$ and $N^+ = 2$ ionization thresholds, respectively. The energy difference between these two thresholds is 2.621 981 748(1) THz [34]. The eigenquantum defects $\mu_{\rm pp}$ and $\mu_{\rm dd}$ are given by the unperturbed quantum defects of the $n{\rm p}1_1$ Rydberg series ($\mu_{\rm pp} = -0.0820$) and the $n{\rm d}2_1$ Rydberg series ($\mu_{\rm dd} = 0.0448$ [30]), respectively. The off-diagonal element $\mu_{\rm pd}$ describes the interaction between the series and its magnitude is a quantitative measure of g/u-symmetry mixing. One should, however, note that Eq. (4) is not an exact description in a system where interaction terms with $\frac{1}{r^2}$, such as an electron-core dipole, play a role. In the case of the Rydberg spectrum of CaF [35] these interactions were also treated in the MQDT framework.

The shifts $\Delta\nu_{g/u}$ of the $n{\rm p}1_1$ Rydberg states resulting from the g/u-symmetry mixing were calculated as a function of $\mu_{\rm pd}$ by solving Eq. (4) and comparing the results to the unperturbed positions obtained by using $\mu_{\rm pd} = 0$. Adjusting $\mu_{\rm pd}$ to minimize the deviation between the calculated shifts $\Delta\nu_{g/u}$ and the observed shifts given in the third column of

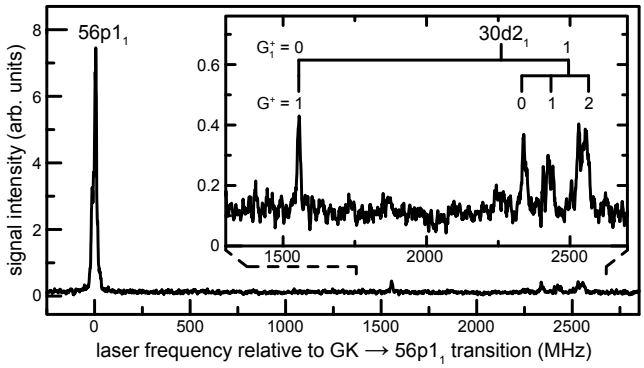

FIG. 7. Observed spectrum in the region of the $GK \rightarrow 56{\rm p}1_1$ transition in HD near 12 675.3 cm^{-1}. Because of g/u-symmetry mixing transitions to the $30{\rm d}2_1$ state are observed (shown on an enlarged scale in the inset). The assignment bars depict the main hyperfine structure of HD^+ taken from Ref. [32].

Table I led to a value $\mu_{\rm pd} = 0.0023(3)$. The corresponding values of $\Delta\nu_{g/u}$ are listed in the fourth column of Table I. Significant shifts of more than 3 MHz result only for the $50p1_1$ and $56p1_1$ Rydberg states which lie closest to members of the perturbing $nd2_1$ Rydberg series (see Fig. 5b). The standard deviation of the final residuals given in the last column of Table I is 2.4 MHz, *i.e.* smaller than the experimental uncertainty. The analysis of the residuals indicates a weak systematic trend from about 2 MHz at $n = 50$ to about -2.5 MHz at $n = 66$. If real, this trend would suggest that the calculated effective quantum defects of the $np1_1$ Rydberg states would be affected by a so far not identified systematic shift of $\sim 1.4 \times 10^{-4}$, which corresponds to 4 MHz at $n = 61$.

The value of $\mu_{\rm pd} = 0.023(3)$ obtained from this analysis can be used to independently estimate the autoionization lifetime of the $61p1_2$ Rydberg state. In the Born-Oppenheimer picture, the $np1_1$ Rydberg series has pure $^1\Pi_u^-$ character while the $np1_2$ has mixed $^1\Sigma_u^+$ and $^1\Pi_u^+$ character. Our MQDT calculations confirm that the $61p1_2$ Rydberg state lies very close to the $np1_1$ Rydberg state (see Fig. 2) and that it has 99 % $^1\Pi_u^+$ character. The autoionization dynamics of the $61p1_2$ Rydberg state is therefore dominated by the same $\mu_{\rm pd}$ interaction element which is responsible for the shifts observed in the $np1_1$ Rydberg series. The autoionization lifetime of the $61p1_2$ Rydberg state predicted by MQDT can be estimated using [33]

$$\tau = \frac{\hbar\nu^3}{4\pi hcR_{\rm HD}\mu_{\rm pd}^2}, \tag{5}$$

where $\nu = n - \bar{\mu} = 61.098$ is the effective principal quantum number with respect to the $N^+ = 1$ threshold. A value of 166(43) ns is obtained for τ, which is of the same order of magnitude as the experimental value (77(10) ns).

F. Observation of $GK\,(v = 1, N = 1) \rightarrow n$g transitions

A further effect of *g/u*-symmetry mixing is observed in the spectrum depicted in Fig. 8. In addition to the transitions to the $64p1_1$ and $64p1_2$ Rydberg states, there are other intense lines present in the spectrum. The structure of these lines corresponds closely to the main hyperfine structure of HD^+, which indicates that the unknown Rydberg state has $\ell > 1$. Our MQDT calculations do not predict any nf Rydberg state to lie in this region and the closest nd Rydberg state with positive total parity is the $31d2_2$ state, which is calculated more than 2 GHz below the region of interest. The center of gravity of the unassigned state

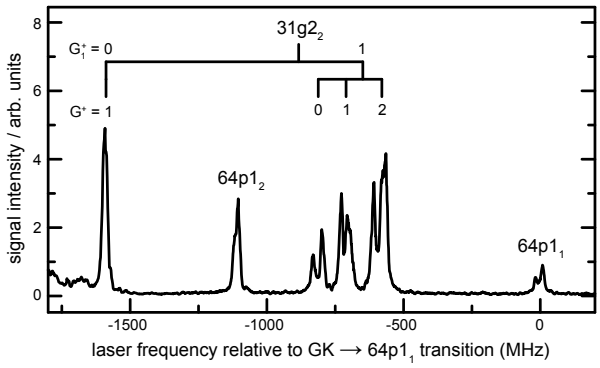

FIG. 8. Observed spectrum in the region of the $GK\,(v=1,N=1) \rightarrow 64\mathrm{p}1_2\,(S=0,v^+=0)$ transition of HD near $12\,683.8\,\mathrm{cm}^{-1}$. Because of g/u-symmetry mixing, transitions to the $31\mathrm{g}2_2$ Rydberg state are observed. The assignment bars depict the main hyperfine structure of HD^+ taken from Ref. [32].

lies at a position which corresponds to an effective principal quantum number of 30.995 with respect to the $N^+=2$ threshold, the quantum defect being only 0.005. Such low quantum defects are typical for nonpenetrating Rydberg states with $\ell > 3$ and we therefore assign the observed lines to the $31\mathrm{g}2_2$ Rydberg state ($\ell = 4$). The high intensities of the observed $GK\,(v=1,N=1) \rightarrow 31\mathrm{g}2_2$ transitions can be explained by g/u-symmetry mixing with the nearby $64\mathrm{f}1_2$ Rydberg states. The $GK\,(v=1,N=1) \rightarrow n\mathrm{f}1_2$ transitions are more than ten times stronger than the transitions to the $n\mathrm{p}1_1$ Rydberg states. The intensity on the low-frequency side of Fig. 8 represents the far wing of the transition to the $64\mathrm{f}1_2$ state. Because the f and g Rydberg states of molecular hydrogen are nonpenetrating the mechanism responsible for the f-g mixing is unlikely to be short-range in nature but must result from the dipolar and higher terms of the multipole expansion fo the core and from core-polarization effects.

G. Precision measurement of the ionization energy of the $GK\,(v=1,N=1)$ state of HD

Our main motivation to excite the high-np Rydberg states of HD from the $GK\,(v=1,N=1)$ state was to carry out a precision measurement of the ionization energy of the $GK\,(v=1,N=1)$ state of HD. The absolute transition frequency of the $GK\,(v=1,N=$

TABLE II. Determination of the $GK\,(v=1,N=1) \rightarrow 61\mathrm{p}1_1\,(S=0,v^+=0)$ transition frequency of HD and error budget (all values in MHz).

	Shift	Uncrt[a]
Transition frequency relative to I_2 reference[b]	−208.1	0.3
Position of the I_2 reference line [25]	380 170 198.5	< 0.1
Pressure shift of the I_2 reference line	−0.4	0.3
Uncertainty of the free spectral range	0.0	< 0.1
Frequency shift in the Ti:Sa amplifier	0.0	0.5
ac Stark shift by the NIR laser	−0.1	0.2
dc Stark shift by residual stray electric field	0.0	0.1
Frequency shift by VIS laser	0.0	0.5
Pressure shift	0.0	< 0.1
Uncertainty of the lineshape model	0.0	0.1
Shift by AOM used in the iodine spectroscopy	−40.0	< 0.1
Shift by AOM used to generate the seed pulse	1000.0	< 0.1
Total[c]	380 170 949.9	0.9

[a] Uncertainty given as one standard deviation.

[b] The transition frequency corresponds to the center of gravity of the hyperfine components.

[c] The total uncertainty was determined by summation of the individual uncertainties in quadrature.

$1) \rightarrow 61\mathrm{p}1_1\,(S=0,v^+=0)$ transition in HD was measured in the same way as in our measurement of the $GK\,(v=1,N=1) \rightarrow 56\mathrm{p}1_1\,(S=0,v^+=0)$ transition in H_2 presented in Ref. [23]. For a detailed description of the systematic shifts and errors we therefore refer to Ref. [23] and only the results are summarized in Table II. The determination was carried out in 10 separate measurements and a statistical analysis leads to a value of 380 170 949.9(9) MHz for the transition frequency of the $GK\,(v=1,N=1) \rightarrow 61\mathrm{p}1_1$ transition in HD.

The ionization energy of the $GK\,(v=1,N=1)$ state is obtained from the $GK\,(v=1,N=1) \rightarrow 61\mathrm{p}1_1\,(S=0,v^+=0)$ transition frequency by adding the electron binding energy of the $61\mathrm{p}1_1\,(S=0,v^+=0)$ Rydberg state, as summarized in Table III. The electron binding energy of the $n\mathrm{p}1_1\,(S=0,v^+=0)$ Rydberg states of HD were determined

TABLE III. Determination of the ionization energy and the term value of the $GK\,(v=1,N=1)$ state of HD. The frequencies and wave numbers correspond to the center of gravity of the hyperfine structure.

Label	Energy interval	Frequency / MHz	Wave number / cm^{-1}	Reference
(1)	$GK\,(v=1,N=1) - 61\mathrm{p}1_1\,(S=0,v^+=0)$	380 170 949.9(9)	12 681.137 89(3)	This work
(2)	$61\mathrm{p}1_1\,(S=0,v^+=0) - X^+\,(v^+=0,N^+=1)$	881 579.9(30)[a]	29.406 34(10)[a]	[26]
(3)[b]	$GK\,(v=1,N=1) - X^+\,(v^+=0,N^+=1)$	381 052 529.8(31)	12 710.544 23(10)	This work
(4)	$X^+\,(v^+=0,N^+=0) - X^+\,(v^+=0,N^+=1)$	1314 925.752(3)	43.861 2019(1)	[34]
(5)[c]	$GK\,(v=1,N=1) - X^+\,(v^+=0,N^+=0)$	379 737 604.0(31)	12 666.683 03(10)	This work
(6)	$X\,(v=0,N=0) - X^+\,(v^+=0,N^+=0)$	3734 469 255(12)	124 568.4858(4)	[20]
(7)[d]	$X\,(v=0,N=0) - GK\,(v=1,N=1)$	3354 731 651(12)	111 901.8028(4)	This work
			111 901.92(10)	[9]

[a] The value determined in Ref. [26] (881 581.7 MHz or 29.406 40 cm^{-1}) was corrected by $-1.8(30)$ MHz (or $0.000\,06(10)\,\mathrm{cm}^{-1}$) (see text for details).

[b] Ionization energy of the $GK\,(v=1,N=1)$ state, determined as (1) + (2).

[c] Adiabatic ionization energy of the $GK\,(v=1,N=1)$ state, determined as (3) − (4).

[d] Term value of the $GK\,(v=1,N=1)$ state, determined as (6) − (5).

in Ref. [26] from high-resolution spectroscopic data by MQDT neglecting g/u-symmetry mixing. The effect of g/u-symmetry mixing was quantified in Section III E and was found to shift the $61\mathrm{p}1_1\,(S=0,v^+=0)$ Rydberg state of HD by $-0.2(1)$ MHz (see Table I). In the same measurement, the systematic trend in the residual deviations between observed and calculated positions of the high-np Rydberg states in the range $n=50$–66 indicated that the calculated electron binding energy of the $61\mathrm{p}1_1\,(S=0,v^+=0)$ Rydberg state of HD might be overestimated by up to 4 MHz. To compensate for this shift an additional correction of $-2.0(30)$ MHz in the binding energy (*i.e.*, of $+2.0(30)$ MHz in the level position) was included in the value used in Table III, resulting in a ionization energy of the $GK\,(v=1,N=1)$ state of HD of $12\,710.544\,23(10)\,\mathrm{cm}^{-1}$.

A new term value of the $GK\,(v=1,N=1)$ state of HD can be obtained from our

measurement when combined with the *ab initio* value of the fundamental rotational spacing of HD^+ from Ref. [34] and the most recent determination of the adiabatic ionization energy of HD presented in Ref. [20] (see Table III). The result ($111\,901.8028(4)\,\mathrm{cm}^{-1}$) is slightly outside the error bar of the experimental result reported by Dabrowski and Herzberg [9] ($111\,901.92(10)\,\mathrm{cm}^{-1}$).

IV. CONCLUSIONS

The following effects of *g/u*-symmetry mixing on both the structure and dynamics of high-n Rydberg states of HD have been observed by high-resolution spectroscopy and under under field-free conditions:

1. np Rydberg states with $N^+ = 1$ were observed to autoionize into the $N^+ = 0$ continuum under emission of a d electron partial wave. The lifetime of the $61p1_2$ Rydberg state was determined experimentally to be $\tau = 77(10)\,\mathrm{ns}$.

2. Transitions from the *gerade* GK $(v = 1, N = 1)$ state to the *gerade* $30d2_1$ and $31g2_2$ Rydberg states could be detected.

3. Shifts of up to 20 MHz were observed for members of the $np1_1$ Rydberg series which lie close to $nd2_1$ Rydberg states. From these shifts, the magnitude of an off-diagonal eigenquantum-defect element $\mu_{\mathrm{pd}} = 0.0023(3)$ of π symmetry could be determined for the singlet Rydberg states.

These different observations are internally consistent, as was verified by estimating the lifetime of the $61p1_2$ Rydberg state using the interaction element $\mu_{\mathrm{pd}} = 0.0023(3)$. The result of $\tau = 166(43)\,\mathrm{ns}$ deviates by two standard deviations from the experimental value, which is likely to have its origin in the approximations made in the present calculations, including the neglect of the hyperfine interaction, of predissociation, and contributions other than those of $^1\Pi$ symmetry to the $61p1_2$ Rydberg state. The fact that the calculated and observed lifetime are of the same order of magnitude confirms, in our opinion, that both the unusual autoionization of the $61p1_2$ Rydberg state and the observed shifts of the $56p1_1$ Rydberg state have their origin in the breakdown of *g/u* symmetry in HD.

The MQDT calculations presented in Ref. [26] of the electron binding energies and the hyperfine structures of singlet $np1_1$ Rydberg states of HD in the range $n = 50$–66 were

validated experimentally. The root-mean-square deviation between observed and calculated positions amounted to 2.3 MHz which is less than the estimated experimental uncertainty of 3 MHz. The analysis of the residual deviations presented in Table I, however, pointed at a systematic error in the calculated electron binding energies of about 4 MHz at $n = 61$.

ACKNOWLEDGMENTS

This work is supported financially by the Swiss National Science Foundation under project 200020-146759 and by the European Research Council advanced grant program under project 228286.

[1] G. Herzberg, *Molecular Spectra and Molecular Structure, Volume I, Spectra of Diatomic Molecules*, 2nd ed. (Krieger Publishing Company, Malabar, 1989).

[2] R. A. Durie and G. Herzberg, Can. J. Phys. **38**, 806 (1960).

[3] M. Trefler and H. P. Gush, Phys. Rev. Lett. **20**, 703 (1968).

[4] P. G. Drakopoulos and G. C. Tabisz, Phys. Rev. A **36**, 5556 (1987).

[5] S. M. Blinder, J. Chem. Phys. **35**, 974 (1961).

[6] L. Wolniewicz, Can. J. Phys. **53**, 1207 (1975).

[7] L. Wolniewicz, Can. J. Phys. **54**, 672 (1976).

[8] K. Pachucki and J. Komasa, Phys. Chem. Chem. Phys. **12**, 9188 (2010).

[9] I. Dabrowski and G. Herzberg, Can. J. Phys. **54**, 525 (1976).

[10] T. Yoshinari, Y. Ogi, and K. Tsukiyama, J. Phys. Chem. A **108**, 7915 (2004).

[11] E. Reinhold, W. Hogervorst, and W. Ubachs, Chem. Phys. Lett. **296**, 411 (1998).

[12] E. Reinhold, W. Hogervorst, W. Ubachs, and L. Wolniewicz, Phys. Rev. A **60**, 1258 (1999).

[13] P. M. Dehmer and W. A. Chupka, J. Chem. Phys. **79**, 1569 (1983).

[14] G. D. Dickenson and W. Ubachs, J. Phys. B: At. Mol. Opt. Phys. **45**, 145101 (2012).

[15] A. de Lange, E. Reinhold, W. Hogervorst, and W. Ubachs, Can. J. Phys. **78**, 567 (2000).

[16] A. de Lange, E. Reinhold, and W. Ubachs, Int. Rev. Phys. Chem. **21**, 257 (2002).

[17] N. Y. Du and C. H. Greene, J. Chem. Phys. **85**, 5430 (1986).

[18] J. M. Gilligan and E. E. Eyler, Phys. Rev. A **46**, 3676 (1992).

[19] G. M. Greetham, U. Hollenstein, R. Seiler, W. Ubachs, and F. Merkt, Phys. Chem. Chem. Phys. **5**, 2528 (2003).

[20] D. Sprecher, J. Liu, Ch. Jungen, W. Ubachs, and F. Merkt, J. Chem. Phys. **133**, 111102 (2010).

[21] K. Chakrabarti, D. R. Backodissa-Kiminou, N. Pop, J. Zs. Mezei, O. Motapon, F. Lique, O. Dulieu, A. Wolf, and I. F. Schneider, Phys. Rev. A **87**, 022702 (2013).

[22] F. Merkt, H. Xu, and R. N. Zare, J. Chem. Phys. **104**, 950 (1996).

[23] D. Sprecher, M. Beyer, and F. Merkt, Mol. Phys. **111**, 2100 (2013).

[24] R. Seiler, Th. Paul, M. Andrist, and F. Merkt, Rev. Sci. Instr. **76**, 103103 (2005).

[25] H. Knöckel, B. Bodermann, and E. Tiemann, (2008).

[26] D. Sprecher, Ch. Jungen, and F. Merkt, Determination of the binding energies of the *np* Rydberg states of H_2, HD and D_2 from high-resolution spectroscopic data by multichannel quantum-defect theory , submitted to *J. Chem. Phys.* (2013).

[27] M. L. Zimmerman, M. G. Littman, M. M. Kash, and D. Kleppner, Phys. Rev. A **20**, 2251 (1979).

[28] R. Patel, N. J. A. Jones, and H. H. Fielding, J. Phys. B: At. Mol. Opt. Phys. **40**, 1369 (2007).

[29] Ch. Seiler, S. D. Hogan, and F. Merkt, Phys. Chem. Chem. Phys. **13**, 19000 (2011).

[30] Th. A. Paul, H. A. Cruse, H. J. Wörner, and F. Merkt, Mol. Phys. **105**, 871 (2007).

[31] A. Osterwalder, A. Wüest, F. Merkt, and Ch. Jungen, J. Chem. Phys. **121**, 11810 (2004).

[32] D. Bakalov, V. I. Korobov, and S. Schiller, Phys. Rev. Lett. **97**, 243001 (2006).

[33] Ch. Jungen, in *Handbook of High-resolution Spectroscopy*, edited by M. Quack and F. Merkt (John Wiley & Sons, Ltd., 2011).

[34] V. I. Korobov, Phys. Rev. A **77**, 022509 (2008).

[35] J. J. Kay, S. L. Coy, B. M. Wong, Ch. Jungen, and R. W. Field, J. Chem. Phys. **134**, 114313 (2011).